

**Title:** Electronic structure of Ce5Rh4Sn10 from XPS and band structure calculations

**Author:** Monika Gamża, Andrzej Ślebarski, H. Rosner

**Citation style:** Gamża Monika, Ślebarski Andrzej, Rosner H. (2008). Electronic structure of Ce5Rh4Sn10 from XPS and band structure calculations. "European Physical Journal B" (Vol. 63, no. 1 (2008), s. 1-9), doi 10.1140/epjb/e2008-00200-4

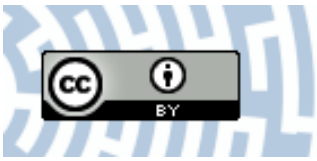

Eur. Phys. J. B **63**, 1–9 (2008)
DOI: 10.1140/epjb/e2008-00200-4

THE EUROPEAN PHYSICAL JOURNAL B

# Electronic structure of $Ce_5Rh_4Sn_{10}$ from XPS and band structure calculations

M. Gamża[1], A. Ślebarski[1], and H. Rosner[2,a]

[1] Institute of Physics, University of Silesia, 40-007 Katowice, Poland
[2] Max Planck Institute for Chemical Physics of Solids, 01187 Dresden, Germany

Received 8 November 2007 / Received in final form 15 April 2008
Published online 28 May 2008 – 

**Abstract.** We present a combined experimental and theoretical study of the electronic structure for the heavy-fermion antiferromagnet $Ce_5Rh_4Sn_{10}$ based on X-ray photoemission spectroscopy (XPS) data and ab initio band structure calculations. The Ce core-level XPS spectra point to a stable trivalent configuration of Ce atoms in $Ce_5Rh_4Sn_{10}$, consistently with both the magnetic susceptibility data and the results of computational structure optimization. The band structure calculations confirm a magnetic ground state with significant magnetic moments only at the Ce atoms. The qualitatively correct description of $Ce^{3+}$ in $Ce_5Rh_4Sn_{10}$ has been achieved using the LSDA+U approach for the Ce $4f$ states. The comparison of the theoretical results with experimental XPS valence band spectrum supports their validity. The calculated partial densities of states suggest that there is a variation in binding energy of the occupied $4f$ states between Ce atoms in nonequivalent crystallographic positions, which is related to the hybridization with Sn states. Finally, the band structure and charge density maps point to the formation of zig-zag chains of the strongly bounded Sn(2), Sn(3) and Rh atoms along the tetragonal axis, whereas Sn(1) shows nearly dispersionless $5s$ bands.

**PACS.** 79.60.-i Photoemission and photoelectron spectra – 71.20.Lp Intermetallic compounds – 71.27.+a Strongly correlated electron systems; heavy fermions

## 1 Introduction

The investigation of the electronic structure of heavy-fermion Ce-based intermetallics is one of the important tasks in the field of strongly correlated electron systems. The main goal of such a study is to improve the understanding of the factors responsible for the formation of the unconventional magnetic, non-magnetic or superconducting ground states in this type of compounds.

In general, the heavy-fermion properties of Ce-based intermetallics can be roughly understood in framework of the Kondo-lattice model [1–4], in which the important parameter is the antiferromagnetic exchange coupling $J_{s-f}$ of the local $f$ moments and the conduction electron states. This coupling gives rise to two competing processes which determine the ground-state properties of Kondo lattices: (i) the on-site Kondo screening of the localized Ce $4f$ moments by the band states, which suppresses the $f$ moments and generate a narrow peak in density of states (DOS) near the Fermi level due to the formation of the Abrikosov-Suhl resonance; (ii) the long range Ruderman-Kittel-Kasuya-Yosida (RKKY) interaction between the local $f$ moments mediated by the conduction electrons. The characteristic temperatures for Kondo effect and RKKY interaction are $T_K \sim \exp(1/\ J_{s-f}N(\epsilon_F))$ and $T_{RKKY} \sim J^2_{s-f}N(\epsilon_F)$, respectively. Here, $N(\epsilon_F)$ is the density of states at the Fermi level. In the strong coupling limit, Ce ions are in an intermediate valence state and the ground state tends to be nonmagnetic. In this case both charge and spin fluctuations play an important role in the physical properties of the materials. For the medium to weak coupling limit, known as the heavy fermion regime, there can be a rich variety of interesting ground states, including complex magnetic structures, reduced moment magnetism, unconventional superconductivity. In this case the charge fluctuations are strongly suppressed and physical properties are governed mainly by the spin fluctuations.

Despite the enormous progress which has been made in the knowledge about heavy-fermion systems, the full solution of the Kondo lattice model and the understanding of the relationship between band structure and the ground state properties in this type of compounds still requires further investigations. Furthermore, it is of great importance to study systems containing several magnetic sites, which can not be characterized by only one coupling parameter and need more sophisticated treatment.

$Ce_5Rh_4Sn_{10}$ is a good example for such a compound. This system forms in the tetragonal $Sc_5Co_4Si_{10}$ structure

[a] e-mail: rosner@cpfs.mpg.de

type, in which the Ce atoms occupy three nonequivalent crystallographic positions. It was claimed to be a moderate heavy fermion antiferromagnet ($\gamma \approx 104$ mJ Ce-mol$^{-1}$ K$^{-2}$) with Néel temperature $T_N \approx 4.3$ K [5].

In this paper we report the results of X-ray photoelectron spectroscopy (XPS) measurements and density functional band structure calculations. Based on the core-level XPS spectra we analyse the valency of Ce ions in $Ce_5Rh_4Sn_{10}$. From the Ce 3$d$ XPS spectrum we estimate the hybridization energy, $\Delta$, using a model based on the Anderson Hamiltonian and developed by Gunnarsson Schönhammer [6]. We argue, that the $\Delta$ parameter can be interpreted as a measure of the *average* hybridization strength between the Ce 4$f$ shell and valence band states in $Ce_5Rh_4Sn_{10}$. In contrast, the band structure calculations give specific information about the electronic structure of Ce in particular crystallographic positions. To get insight into the chemical bonding in $Ce_5Rh_4Sn_{10}$ we analyse the valence and difference charge density maps. We performed also the computational crystal structure optimization. We provide the fully optimized lattice parameters and the atomic coordinates, since the internal atomic positions for $Ce_5Rh_4Sn_{10}$ were not reported so far.

Recently we have found that some compounds of the series of Ce-Rh-Sn intermetallics shows the sign of spin fluctuations owing to the Rh 4$d$ electrons [7,8]. In order to investigate the possible spin fluctuations on Rh atoms in $Ce_5Rh_4Sn_{10}$ we have carried out ac magnetic susceptibility measurements down to a temperature of 2 K.

## 2 Methods

### 2.1 Experimental

A polycrystalline sample of $Ce_5Rh_4Sn_{10}$ was prepared by arc melting of the elemental metals (Ce 99.99%, Rh 99.95%, Sn 99.995%, in units of atomic %) in the ratio 5:4:10 on a water cooled cooper hearth in an ultra-high purity Ar atmosphere with an Al getter (heated above the melting point). The sample was remelted several times to promote homogeneity and annealed at 800 °C for 7 days. The quality of the sample was examined by X-ray powder diffraction (XRD) analysis. The measurements were performed on a Siemens D-5000 diffractometer using Cu $K_\alpha$ radiation. The XRD patterns analysis revealed that the $Ce_5Rh_4Sn_{10}$ crystallizes in the tetragonal $Sc_5Co_4Si_{10}$ structure type, consistently with previous results [5,9]. The sample was found to be in good quality. Only few additional very slight Bragg peaks were detected, which we assign to a small amount of an unidentified minority phase. The lattice parameters acquired from the diffraction patterns analysis (Tab. 1) are in agreement with those previously reported [5,9]. We tried to synthesize also the reference compound $La_5Rh_4Sn_{10}$, but we didn't succeed. This outcome is consistent with analysis performed by Venturini et al. [9], who found that $La_5Rh_4Sn_{10}$ is out of stability range for stannides which crystallize in the $Sc_5Co_4Si_{10}$ type of structure.

**Table 1.** Crystal structure data for $Ce_5Rh_4Sn_{10}$ compound. The calculated lattice parameters and internal positions were rounded to 3 significant digits.

| Lattice parameters | $a$ (Å) | $c$ (Å) | | |
|---|---|---|---|---|
| experiment | 14.049 | 4.620 | | |
| experiment [9] | 14.053 | 4.621 | | |
| LDA | 13.935 | 4.526 | | |
| Atomic positions (LDA) | | $x$ | $y$ | $z$ |
| Ce(1) | 2a | 0 | 0 | 0 |
| Sn(1) | 4g | 0.069 | 0.569 | 0 |
| Ce(2) | 4h | 0.176 | 0.676 | 0.5 |
| Ce(3) | 4h | 0.388 | 0.888 | 0.5 |
| Rh | 8i | 0.253 | 0.526 | 0 |
| Sn(2) | 8i | 0.157 | 0.198 | 0 |
| Sn(3) | 8j | 0.162 | 0.003 | 0.5 |

The XPS spectra were obtained with monochromatized Al $K_\alpha$ radiation at room temperature using a PHI 5700 ESCA spectrometer. The overall energy resolution was about 0.4 eV. The polycrystalline sample was broken in a high vacuum of $6 \times 10^{-10}$ Torr immediately before taking spectra. The photoelectrons were taken almost vertically. The calibration of the spectra was performed according to reference [10]. Binding energies were referenced to the Fermi level ($\epsilon_F = 0$).

The ac magnetic susceptibility was measured in the temperature range of 1.8–300 K using a commercial ac Lake-Shore susceptometer. The amplitude of the excitation field was 1 mT at a fixed frequency of 10 kHz.

### 2.2 Computational

The electronic structure of the compound $Ce_5Rh_4Sn_{10}$ was studied using the Full Potential Local Orbital (FPLO) Minimum Basis code (version 5.00-19) [11] within the local spin density approximation (LSDA). In the scalar-relativistic calculations the XC potential of Perdew and Wang was employed [12]. As basis set, Ce(4$f$5$s$5$p$/5$d$6$s$ 6$p$), Rh(4$s$4$p$/4$d$5$s$5$p$) and Sn(4$s$4$p$4$d$/5$s$5$p$:5$d$) states were employed as semi-core/valence:polarization states. The lower-lying states were treated fully relativistically as core states. The inclusion of semi-core states was forced by their non-negligible overlap due to the large extension of their wave functions. The Sn 5$d$ states were taken into account as polarization states to improve the completeness of the basis set. The spatial extension of the basis orbitals, controlled by the confining potential exponent equal to 5, was optimized to minimize the total energy [13]. The strong Coulomb correlation within the Ce 4$f$ shell was treated in a mean field approximation using the LSDA+U method [14] (applying the around mean field double counting scheme). The Coulomb repulsion $U$ and exchange constant $J$ for the 4$f$ states of all three types of Ce atoms were assumed to be 4–7 eV and 0–0.7 eV, respectively. Within this range of parameters, no significant changes of the electronic structure apart from the exact position of

the Ce $4f$ levels were observed. A $k$-mesh of 120 points in the irreducible part of Brillouin zone (916 in the full zone) was used.

To analyse the topology of the valence charge density as well as atomic forces we performed also band structure calculations by the Full Potential Linearized Augmented Plane-Wave (FP-LAPW) method [15] using WIEN2k_05 computer code [16]. The resulting electronic densities of states and band structures were basically identical for the two band structure codes.

Based on the band structure results we estimated the theoretical XPS valence band spectra. The partial $l$-resolved densities of states were multiplied by the corresponding cross sections [17]. The results were multiplied by the Fermi-Dirac function for 300 K and convoluted by the Lorentzians with a full width at half maximum (FWHM) of 0.4 eV to account for the instrumental resolution, thermal broadening and the effect of the lifetime of the hole states.

## 3 Results and discussion

### 3.1 Ce core-level XPS spectra

The most intensive peaks in Ce XPS spectra are related to photoemission from Ce $3d$ and $4d$ states.

Figure 1 shows the Ce $3d$ XPS spectrum for the compound $Ce_5Rh_4Sn_{10}$. Due to the spin-orbit (SO) interaction there are two sets of Ce $3d$ photoemission lines in the spectrum assigned to the $3d_{3/2}$ and $3d_{5/2}$ components of the final states, with an intensity ratio $I(3d_{5/2})/I(3d_{3/2}) = 3/2$. The estimated value of the SO splitting ($\delta \approx 18.6$ eV) is in agreement with that obtained from the ab initio calculations ($\delta \approx 18.84$ eV) for all Ce atoms in $Ce_5Rh_4Sn_{10}$.

The main photoemission lines originating from $Ce^{3+}$ are labelled as $f^1$. The lowest energy components marked as $f^2$ appear owing to the strong Coulomb interaction between photoemission hole in core shell and electrons located near the Fermi level. These contributions originate from a screening of the core hole by electrons from the valence band to the $4f$ states, which is possible due to hybridization of the Ce $4f$ shell with conduction band states. Therefore the $f^2$ peak intensity with respect to the sum of the intensities of the $f^1$ and $f^2$ peaks can be considered as an indicator of the hybridization strength [18]. In the investigated energy range the Ce $3d$ photoemission lines overlap with a small peak due to the Sn $3s$ states which is located at about 885 eV. In the Ce $3d$ XPS spectrum we found also some broad features at binding energies of 897.1 eV, 909.6 eV and 915.7 eV. We interpret these features as plasmon resonance structures which arise from collective oscillations of the conduction electrons, that we indicated in Figure 1. The plasmon energy, i.e. the energy interval between the main peak and the loss line, was found to be about 12.5 eV. We note that very similar energy loss structures have been observed recently in the Ce $3d$ XPS spectrum of $CeRhSn_2$ [7]. There are no additional, sharp peaks in the Ce $3d$ XPS spectrum in a range of ~11 eV from the main photoemission lines which could

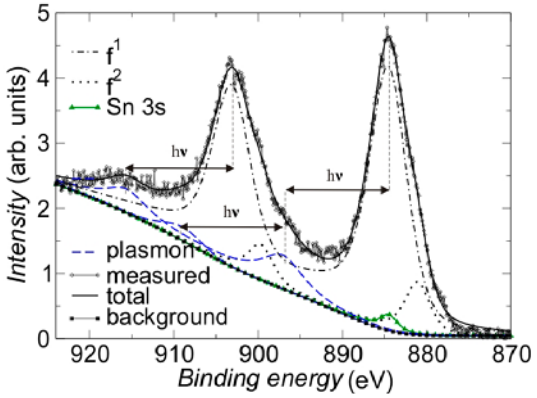


**Fig. 1.** The Ce $3d$ XPS spectrum for $Ce_5Rh_4Sn_{10}$ deconvoluted based on the Gunnarsson and Schönhammer theoretical model [6]. The plasmon energy h$\nu$ (~12.5 eV) is marked by arrows.

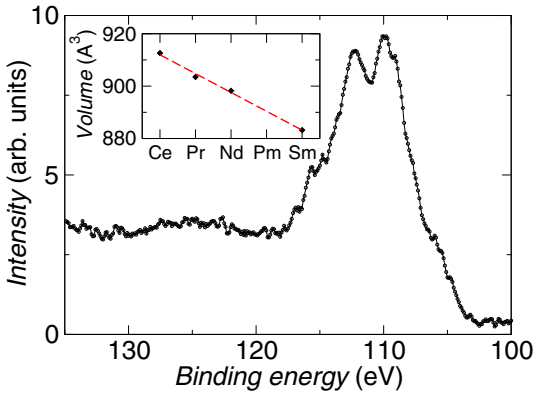


**Fig. 2.** The Ce $4d$ XPS spectrum for $Ce_5Rh_4Sn_{10}$. The inset shows the comparison of the unit cell volumes, calculated from the experimental lattice parameters, for the series of $RE_5Rh_4Sn_{10}$ intermetallics (RE–rare earth element). Both plots point to a stable trivalent configuration of Ce atoms in $Ce_5Rh_4Sn_{10}$.

be assigned to the Ce $3d^9f^0$ final state, giving an evidence of an intermediate valence behavior of Ce in the system $Ce_5Rh_4Sn_{10}$.

The valence of Ce ions close to 3+ has also been confirmed by the Ce $4d$ XPS spectrum (Fig. 2), where one can observe only a broad structure at binding energies ranging from 104 eV to 117 eV. This complex originates from two sets of photoemission lines whose separation corresponds to the core-hole $4d$ spin-orbit interaction and equals to ~3.2 eV. These peaks are assigned to the $4d^94f^1$ and $4d^94f^2$ final states. The shape of this region, however, can not be interpreted in detail because of the $4d$-$4f$ interaction which is much stronger than the $3d$-$4f$ coupling and introduces strong multiplet effects [19]. In Ce $4d$ XPS spectra for the intermediate valence systems there are additional photoemission lines due to the $4d^94f^0$ final states. These peaks are usually observed in a distance of ~11 eV from the main peaks and their splitting is almost equal to the $4d$ spin-orbit splitting in La (~2.9 eV) [18–20]. In the Ce $4d$ XPS spectrum of $Ce_5Rh_4Sn_{10}$ there is no

evidence for additional sharp peaks at a binding energy of 118–124 eV, which would provide evidence of an intermediate valence behavior of Ce. There appears only a broad feature in a distance of 12–13 eV from the main photoemission structure, which we interpret as plasmon-loss satellite. Similar plasmon-like features were found recently in Ce $4d$ XPS spectra of $CeRhSn_2$ [7].

In order to estimate the hybridization strength between the $4f$ and conduction band states we performed the quantitative analysis of the Ce $3d$ XPS spectra based on the Gunnarsson and Schönhammer (GS) model calculations [6,18]. The $\Delta$ parameter, which describes the hybridization strength between the Ce $4f$ shell and conduction electron states, is defined as $\pi V^2 \rho_{max}$, where $\rho_{max}$ is the maximum value of the DOS and $V$ is the hybridization matrix element in the Anderson impurity Hamiltonian. The $\Delta$ value was estimated using Figures 5 and 6 of the reference [18], assuming the conduction band's DOS to be a simple semielliptic with lower edge $B^- = -4$ eV and upper edge $B^+ = 1.57$ eV with respect to the Fermi level. The other parameters in the GS model were assumed to take values typical for Ce-based intermetallics (the Coulomb interaction between the core hole and the $4f$ subshell $U_{fc} \cong 9.6$–$13.0$ eV and the Coulomb interaction between the $4f$ electrons $U_{ff} = 6.4$ eV). The separation of the overlapping peaks in the spectrum was done on the basis of the Doniach-Šunjić theory [21]. A background, calculated using the Tougaard algorithm [22] was subtracted from the XPS data. Such an estimation yielded $\Delta \approx 50$ meV.

The estimated $\Delta$ value we interpret as the *average* hybridization energy for the Ce atoms which occupy three nonequivalent crystallographic positions in $Ce_5Rh_4Sn_{10}$, since the measured Ce XPS spectra contain the total signal from all of the Ce atoms. It is worthwhile to underline that the ab initio band structure calculations revealed the differences in binding energy between crystallographically nonequivalent Ce atoms of the order of 0.2–0.6 eV, depending on the applied method (FPLO or LAPW) and approximation (LDA, LSDA, LSDA+U). These shifts are much smaller than the intervals between the $f^1$ and $f^2$ contributions, which justifies the interpretation of the estimated $\Delta$ as an averaged value.

There are several possible sources of error in the estimation of the $\Delta$ value. One of the most important is the surface contribution to the measured spectra. Since the inelastic mean free path for the photoelectrons with kinetic energy of 600 eV is about 10 Å [23], approximately 20% of the XPS spectrum arises from the first atomic layer where Ce might have different electronic structure. Besides, significant uncertainties are related also to the spectra decomposition and the background subtraction.

It is worthwhile to point out that the assumed theoretical model does not include the dependence of the hybridization parameter $\Delta$ on the Ce $4f$ configuration [24,25]. The creation of a deep core hole in photoemission process should modify the distribution of the $4f$ charge around the Ce atoms, resulting in a shrinking of the $4f$ wavefunction. This effect may lead to a smaller hybridization strength in final state as compared with the ground state. Witkowski et al. [24] have modified the Anderson model and introduced two hybridization parameters into the Hamiltonian to account for the influence of the core hole on the hybridization coupling in the final state. Their comparison of the theoretical results with the experiment suggests that configuration dependence of the hybridization strength is important for strongly-hybridized systems, while for systems with medium and weak hybridization this effect is not significant.

Finally, the GS model gives zero-temperature spectral functions, whereas the experimental spectra were collected at room temperature. A disagreement between zero-temperature calculations and our measurements could result from the temperature dependence of the spectral function. However, the experimental data for other Ce based intermetallics indicate that this dependence for the core-levels is small [24].

The estimated hybridization energy $\Delta$ for $Ce_5Rh_4Sn_{10}$ is much smaller than the typical values for intermediate valence compounds (100–160 meV) [18,26,27], which corroborates with the occupation of the $4f$ shell close to one for all Ce atoms in $Ce_5Rh_4Sn_{10}$. This result, together with thermodynamic data [5], indicates that the compound $Ce_5Rh_4Sn_{10}$ belongs to the heavy fermion regime of the Kondo lattice model.

It is worth noting that similar $\Delta$ value ($\sim$60 meV) was found recently for another antiferromagnetic Kondo lattice compound, $CeIn_3$, which has attracted great interest due to the superconducting transition via a heavy fermion state at the pressure of $\sim$ 2.6 GPa [28,29]. This unusual superconducting state is believed to be characterized by magnetically mediated Cooper pairing. In this regard it is of immediate importance to study in detail the electronic structure of the compound $Ce_5Rh_4Sn_{10}$ as well as its response to applied pressure in order to get insight into the factors responsible for the formation of the unconventional ground states in heavy fermion systems.

### 3.2 Structure optimization

The compound $Ce_5Rh_4Sn_{10}$ was found to crystallize in the tetragonal structure of the $Sc_5Co_4Si_{10}$-type [9]. The experimental lattice parameters are listed in Table 1. The comparison of the unit cell volumes for the series of $RE_5Rh_4Sn_{10}$ intermetallics (Fig. 2) strongly indicates that the Ce atoms in $Ce_5Rh_4Sn_{10}$ are in a trivalent state, which is in agreement with the XPS spectra. Since no exact atomic coordinates were reported so far, we performed a full structure optimization based on the electronic band structure calculations within the LDA approximation. As a starting point we took atomic positions for the isostructural $Nd_5Rh_4Sn_{10}$ compound [9] and the experimental lattice parameters (Tab. 1) estimated for polycrystalline $Ce_5Rh_4Sn_{10}$. The resulting lattice parameters and atomic positions are listed in Table 1. We cross-checked the FPLO results using the WIEN2k_05 computer code, where the atomic forces were calculated according to the method

**Table 2.** DOS($\epsilon_F$), Sommerfeld coefficient $\gamma$ and spin moments $M$ of Ce(1), Ce(2) and Ce(3) calculated for the $Ce_5Rh_4Sn_{10}$ compound within different approximations for the XC potential.

| | LDA | LSDA | LSDA+U (U ∼ 6 eV) |
|---|---|---|---|
| DOS($\epsilon_F$) (states $eV^{-1}$f.u.$^{-1}$) | 53.9 | 30.0 | 9.5 |
| $\gamma$ (mJ Ce-mol$^{-1}$K$^{-2}$) | 25.4 | 14.1 | 4.5 |
| $M_{Ce(1)}$ ($\mu_B$) | - | 0.02 | 1.01 |
| $M_{Ce(2)}$ ($\mu_B$) | - | 0.25 | 0.93 |
| $M_{Ce(3)}$ ($\mu_B$) | - | 0.81 | 1.01 |

proposed by Yu et al. [30] For the optimized atomic positions we got total forces on each atom smaller than 10 mRy/a.u. It is worthwhile to stress that the theoretical lattice parameters are in good agreement with the experimental ones. It suggests that the Ce $4f$ states do not contribute significantly to the chemical bonding in $Ce_5Rh_4Sn_{10}$.

### 3.3 Valence band of $Ce_5Rh_4Sn_{10}$

Figure 3 shows the total DOS for $Ce_5Rh_4Sn_{10}$ calculated within the LSDA approximation. The spin-polarized band structure calculations confirm a magnetic ground state with significant magnetic moments only at the Ce atoms (Tab. 2), in agreement with the experimental results. The LSDA approach, however, results in unrealistic partial $4f$ contributions to the DOSs forming narrow peaks at the Fermi level due to the large underestimation of the Coulomb correlation within the Ce $4f$ shell in the LSDA approach. To account for the strong Coulomb repulsion in a mean field like (static) approximation we performed additional band structure calculations using the so-called LSDA+U method. The application of this method to the Ce $4f$ states leads to a shift of the occupied Ce $4f$ bands toward higher binding energies and of the unoccupied $4f$ states above the Fermi level. Consequently, it removes the incorrect hybridization with conduction states and yields the qualitatively correct physical picture of Ce in a trivalent state with the occupied and the unoccupied Ce $4f$ states split of the order of $U$–$J$. Thus, the magnetic spin moments for Ce atoms in all nonequivalent positions are about 1 $\mu_B$. The spin moments on Rh and Sn calculated using the LSDA+U approach are below 0.01 $\mu_B$. This suggests that the long range antiferromagnetic ordering at low temperatures can be attributed, in a first approximation, to the RKKY interaction among the local $f$ moments, which is transferred via the conduction electrons. The magnetic structure of the $Ce_5Rh_4Sn_{10}$ compound is supposed to be complicated, since in the crystal structure there are three nonequivalent crystallographic positions occupied by magnetic Ce atoms. The analysis of band structure (Fig. 4) clearly shows that the dispersion out of plane (along $\Gamma$–Z) is significantly larger than that in-plane (along $\Gamma$–X–M–$\Gamma$), especially for the Sn(2) and Sn(3) states. This suggests that the main direction for the

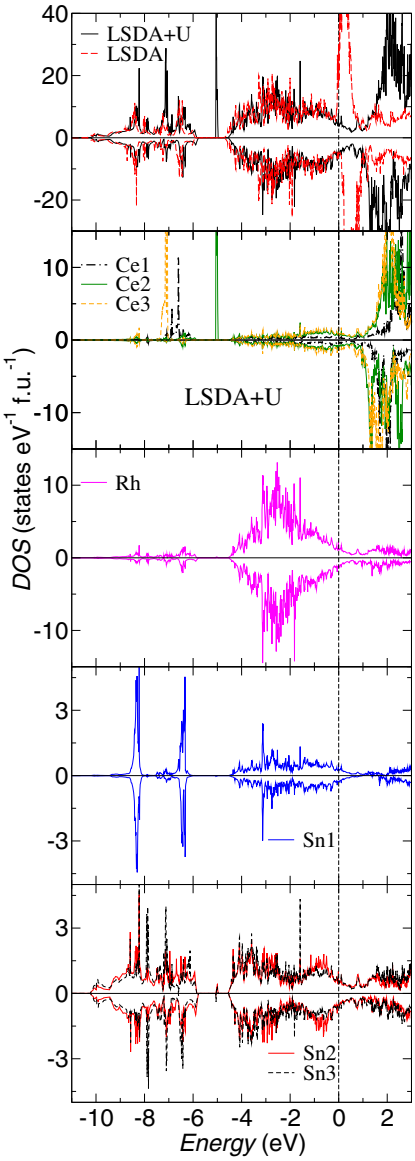


**Fig. 3.** The comparison of the total DOSs calculated within the LSDA and LSDA+U ($U$ = 6 eV) approximation and the atom projected DOSs obtained using the LSDA+U approach. The majority (minority) spin was plotted upward (downward). The common vertical dash line indicates the position of the Fermi level.

RKKY-type magnetic interactions is along the tetragonal axis. Obviously further investigations, including neutron scattering experiments, should be carried out to improve the understanding of the magnetism in $Ce_5Rh_4Sn_{10}$.

The total and partial atomic resolved DOSs calculated within the LSDA+U approximation are shown in Figure 3. For all nonequivalent Ce atoms the values for the $U$ and $J$ parameters were varied in ranges of 3–7 eV and 0–0.7 eV, respectively. In the applied range of the $U$ and $J$ values the shape of the electronic DOS for all atoms except Ce is almost independent on the choice of these parameters. Moreover, there are no noticeable changes in the DOSs in the region close to the Fermi level, which is crucial for

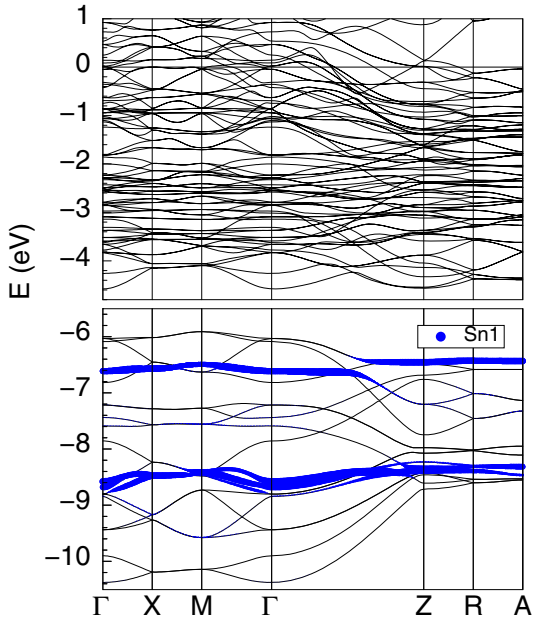


**Fig. 4.** Band structure of $Ce_5Rh_4Sn_{10}$ calculated within the LSDA+U approximation. For the upper panel the $U$ and $J$ parameters were assumed to take values 6 eV and 0 eV, respectively, for all Ce atoms, while for the lower panel they were assumed to be 4 eV and 0 eV, respectively. The high symmetry points are labelled according to the standard notation.

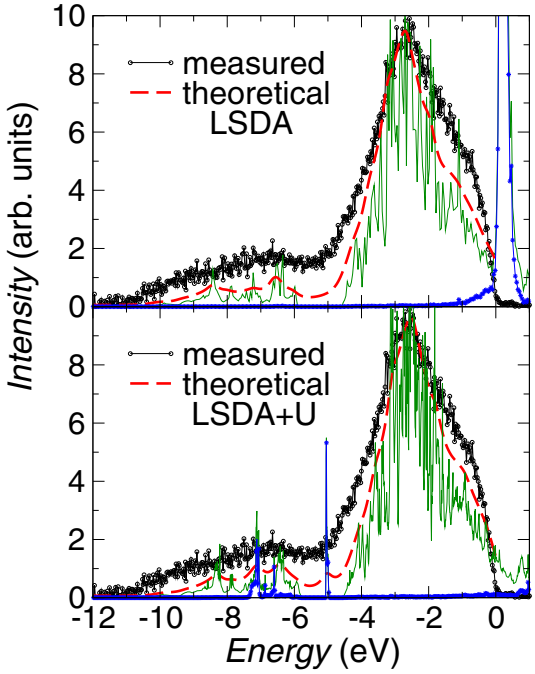


**Fig. 5.** The comparison of the XPS valence band spectrum of $Ce_5Rh_4Sn_{10}$ (background subtracted) with the calculated ones based on the densities of states obtained within the LSDA approximation and using the LSDA+U ($U = 6$ eV) approach for the strong Coulomb interactions within the Ce $4f$ shell for each Ce atom. The thin grey (green) solid lines represent the sum of the partial l-resolved DOSs multiplied by the corresponding cross sections. The thin (blue) solid lines with (blue) stars show the sum of the partial Ce(1), Ce(2) and Ce(3), respectively, $4f$ DOSs multiplied by the photoemission cross section.

the low-lying excitations. This justifies the application of the LSDA+U approximation, although the real values of $U$ and $J$ parameters may vary slightly for Ce atoms in all three nonequivalent positions.

It is worth noting that only in case of Ce(2) the occupied and unoccupied $4f$ states show a split of the order of ($U$-$J$). For Ce(1) and Ce(3) the distance between the occupied and unoccupied $f$ states is significantly larger (∼1.5 eV), which we assign to the hybridization with Sn states. This interpretation is consistent with observation that for the reference $La_{2.5}Y_{2.5}Rh_4Sn_{10}$ compound the RE(2) (RE - rare earth element) crystallographic position is almost exclusively occupied by the smaller $Y^{3+}$ ions [31]. The larger $La^{3+}$ ions, comparable in size with the $Ce^{3+}$ ions, fill in the RE(1) and RE(3) positions, where they can form covalent bonds with the NN Sn(2) and Sn(3) atoms.

The typical value of the $U$ parameter for Ce in a trivalent state was calculated to be about 5–7 eV [32]. The ab initio estimates has been confirmed by experimental results [33]. For the investigated compound $Ce_5Rh_4Sn_{10}$, application of the $U$ parameter equal to 6 eV results in the occupied $f$ bands at binding energies of 6.7 eV, 5 eV and 7 eV for Ce1, Ce2 and Ce3, respectively. On the other hand, a large number of photoemission experiments for different Ce-based systems unanimously revealed that for the compounds located in the heavy fermion regime the ionization energy of the Ce $4f$ level is of 2–4 eV [34]. The typical position of the Ce $4f$ photoionization peaks has been reproduced in our band structure calculations for $Ce_5Rh_4Sn_{10}$ assuming that the $U$ parameter is about 3 eV. One should note, however, that the $4f$ signal in photoelectron spectra originates from the final state after photoemission and corresponds to the removal of an $f$ electron with simultaneous screening by electrons close to the Fermi level. Thus, its position in binding energy depends also on the screening of the $f$ hole by conduction electrons.

To analyse the XPS valence band spectrum of $Ce_5Rh_4Sn_{10}$ we have estimated the theoretical XPS spectra based on the calculated partial DOSs, according to the description in Section 2.2. The exemplary results obtained from the DOSs calculated within the LSDA and LSDA+U ($U = 6$ eV) approximation are presented in Figure 5. The theoretical XPS spectra fit well to the experimental data, which confirms the reliability of our band structure calculations. The most intense peak in valence band spectrum located at about 2.5 eV originates mainly from the Rh $4d$ states hybridized with $5p$ states of Sn. The second peak centered at about 7 eV is related to photoemissions from Sn $5s$ states. To expose the Ce $4f$ contributions to the XPS valence band spectrum we plotted also the partial Ce $4f$ DOSs as well as the sum of all partial l-resolved DOSs, multiplied by the corresponding cross-sections (Figs. 5a, 5b). Since the Ce $4f$ give only small contributions to the XPS valence band as compared to the other valence band states, the experimental XPS spectrum is not decisive with

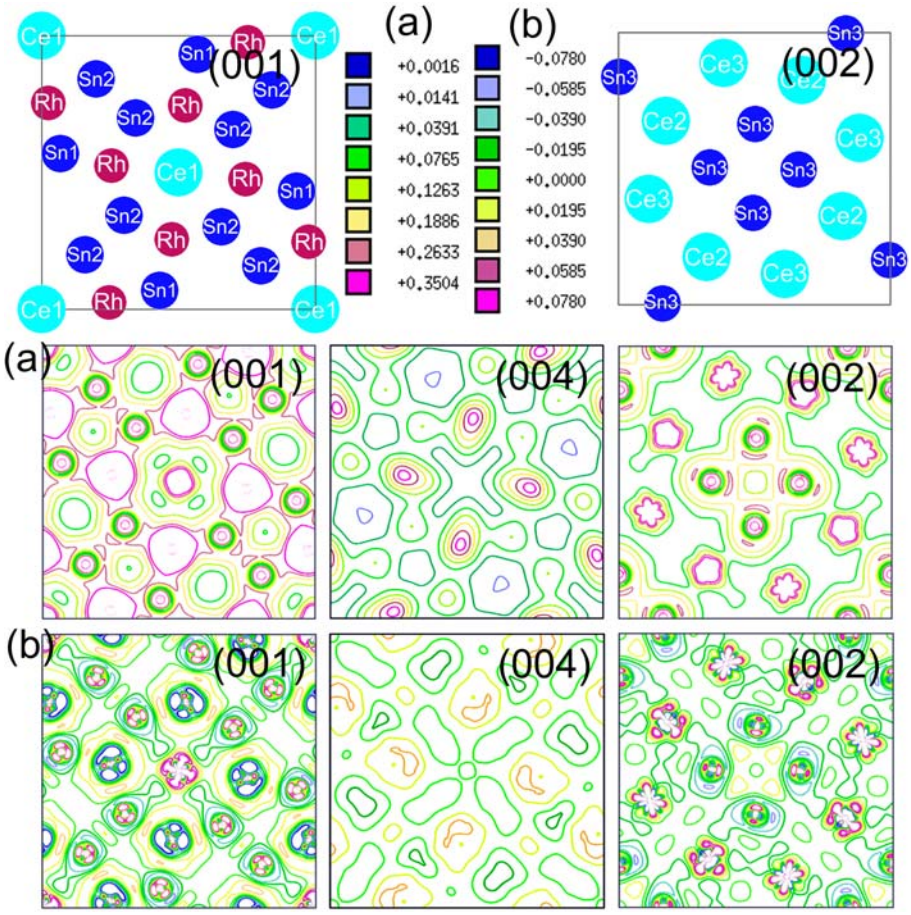


**Fig. 6.** Total valence (a) and difference (b) charge densities (electron/Å$^3$) for the planes (001), (002) and (004) of $Ce_5Rh_4Sn_{10}$ provided with legends. The charge density maps reveal the strongest charge accumulations located between Rh and Sn(3) atoms as well as around the middlepoint of the unit cell. The former point to the covalent-like bonds between Rh and Sn(3) atoms, while the latter are strongly elongated toward the nearest neighbour Sn(2) atoms suggesting the formation of the multi-center bonds for the Sn(3) and Sn(2) atoms.

respect to the localization of the $4f$ states in valence band. Further experimental studies are required to clarify the energy position of the $4f$ bands for $Ce_5Rh_4Sn_{10}$.

The calculated values of the DOS at the Fermi level and the Sommerfeld coefficients are listed in Table 2. We note that the experimental $\gamma$ value estimated from the fit of the low temperature specific heat data equals to 104 mJ Ce-mol$^{-1}$ K$^{-2}$ [5] and is of one order of magnitude larger than the theoretical bare values obtained from the DOS($\epsilon_F$) (Tab. 2). Different effects, e.g., phonon-electron coupling or low-lying magnetic excitations can enlarge the $\gamma$ value. The strong enhancement, however, suggests that in low temperatures there is a peak of the electronic quasi-particle DOS at the Fermi level originating from an Abrikosov-Suhl resonance. It is worthwhile to stress that the LSDA+U approach is a static mean-field approximation. Consequently, this method can not account for the dynamic correlation effects, which are responsible for the heavy-fermion properties of Ce-based intermetallics. The XPS valence band spectrum recorded at room temperature also can not give the clear evidence for the Abrikosov-Suhl resonance in $Ce_5Rh_4Sn_{10}$, since based on the thermodynamic measurements [5] the Kondo temperature for this compound should be very low and in higher temperatures the resonance therefore vanishes.

A surprising feature in the band structure of $Ce_5Rh_4Sn_{10}$ is the shape of the Sn(1) $5s$ states. These states are split into two groups of bands, which exhibit only a small dispersion (Fig. 4). Thus they contribute to the two very narrow, well separated peaks in the electronic DOS of Sn(1) located at about 6.5 eV and 8.3 eV (Fig. 3). In contrast, $5s$ states of Sn(2) and Sn(3) strongly hybridize with each other, forming common bands with considerable Rh $4d$ contribution. These bands shows a significant dispersion mainly along the tetragonal axis ($\Gamma$–Z). Such a band structure points to the formation of vertical zig-zag chains containing strongly bounded Sn(2), Sn(3) and Rh atoms. To gain deeper inside into the bondings in $Ce_5Rh_4Sn_{10}$ we analyse charge density distribution.

### 3.4 Charge density analysis

The calculated *valence charge densities* in planes (001), (002) and (004) for the compound $Ce_5Rh_4Sn_{10}$ are presented in panels (a) of Figure 6. In order to visualize the

reordering of electronic charge density accompanying the bonding formation, the *difference charge densities* were obtained by subtracting the superposition of free atom densities from the total *valence charge density*. The results are shown in panel (b) of Figure 6.

$Ce_5Rh_4Sn_{10}$ forms in a layered structure. Therefore, looking only at the crystal structure one could expect the strong bonds within the Ce(1)-Rh-Sn(1)-Sn(2) and the Ce(2)-Ce(3)-Sn(3) layers. Instead, we found the strongest charge accumulations distributed between the (001) and (002) planes, which suggests the formation of covalent-like bonds along the tetragonal axis. The most pronounced charge accumulations are located between Rh and Sn(3) atoms as well as around the middlepoint of the unit cell. The last ones are strongly elongated toward the nearest neighbouring (NN) Sn(2) atoms suggesting the formation of the multi-center bonds for the Sn(3) and Sn(2) atoms. These results point to the formation of zig-zag chains of strongly bounded Sn(2), Sn(3) and Rh atoms in the investigated crystal structure, consistently with our band structure analysis. Meanwhile the Sn(1) atoms are surrounded only by the slight charge accumulations distributed between the Sn(1), Ce(2), Ce(3) and Rh atoms and between the pairs of the NN Sn(1) atoms. The latter dimer-like feature is inline with the almost dispersionless Sn(1) 5$s$ bands in Figure 4 (at 6.6 eV and 8.5 eV).

It worth noting that the topology of the valence and difference charge densities is the same for LSDA and LSDA+U calculations and does not depend on the values of the $U$ and $J$ parameters applied for Ce 4$f$ states in LSDA+U approach. The picture derived from charge density distribution has been also confirmed by the electron localization function (ELF) analysis [35].

### 3.5 Magnetic susceptibility

The temperature dependence of the magnetic susceptibility for the compound $Ce_5Rh_4Sn_{10}$ is shown in Figure 7. There is a sharp peak in the susceptibility curve at about 4.1 K, giving a clear evidence of an antiferromagnetic ordering. It is consistent with previous reports, which pointed to a bulk magnetic phase transition at the temperature of 4.4 K [5]. The temperature dependence of the susceptibility measured up to 300 K does not exhibit any feature which could be attributed to charge or spin fluctuation effects. This result confirms the stable valency of the Ce ions in $Ce_5Rh_4Sn_{10}$ and rules out the possibility of spin fluctuations owing to Rh 4$d$ electrons in this compounds.

## 4 Conclusions and summary

To summarize, we presented a joined experimental and theoretical study of the electronic structure of $Ce_5Rh_4Sn_{10}$ using XPS and density functional band structure calculations. The Ce core-level XPS spectra show clearly a stable $Ce^{3+}$ configuration. This is in line with our susceptibility data. They also point to a magnetic phase transition at $T_N \approx 4.4$ K. A magnetic ground state is supported by our band structure calculations. We find significant magnetic moments only at the Ce sites, whereas Rh and Sn atoms are nearly unpolarized. The stable $Ce^{3+}$ valence is collaborated by the result of the computational structure optimization which yields a volume that is only slightly smaller than the experimental one from the X-ray powder diffraction analysis. In addition, the atomic coordinates have been fully optimized resulting in internal positions similar to that for the related $Nd_5Rh_4Sn_{10}$ [9]. Moreover, the volume of $Ce_5Rh_4Sn_{10}$ obeys according to Vegard's law assuming a $Ce^{3+}$ state. The validity of our band structure calculations is supported by the comparison of the XPS valence band spectra with the calculated partial DOSs taking into account the corresponding atomic-like cross sections and the experimental resolution. We find a good agreement between the measured spectra and the spectra estimated from the DOSs using the LSDA+U as a mean field like approximation for the strong electron correlations in the Ce 4$f$ shell. An analysis of the chemical bonding has been provided based on electron density and difference density maps.

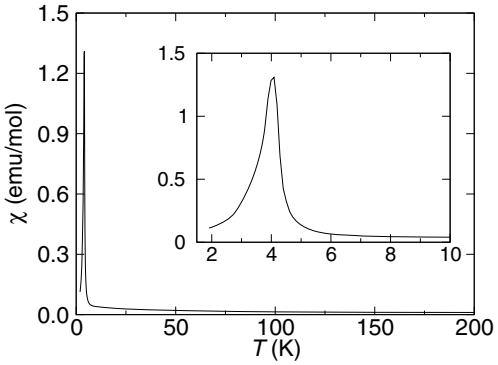


**Fig. 7.** The ac magnetic susceptibility of $Ce_5Rh_4Sn_{10}$.

The presented results support the generally accepted picture that for heavy fermion systems the valence of Ce ions is close to 3+ and the differences in ground state properties result first of all from the interplay between the coupling of the 4$f$ and conduction band states ($\Delta$) and the intra-atomic Coulomb interaction among the localized 4$f$ states, as discussed previously [4].

The authors thank Marek Kulpa for help with XPS experiments and K. Wagner for the ELF analysis. The authors also thank for financial support from Projects No. 1 P03B 052 28, No. N202 010 32/0487 of Ministry of Science and Higher Education and for the DFG, Emmy Noether-program.

## References

1. S. Doniach, Physica B **91**, 231 (1997)
2. J.R. Iglesias, C. Lacroix, B. Coqblin, Phys. Rev. B **56**, 11820 (1997)
3. M. Loewenhaupt, K.H. Fischer, *Handbook on the Physics and Chemistry of Rare Earths*, edited by K.A. Gschneider Jr., L. Eyring (1993),Vol. 16, Chap. 105
4. A.C. Hewson, *The Kondo Problem to Heavy Fermions* (Cambridge University Press, Cambridge, 1993)

5. N.G. Patil, S. Ramarkrishnan, Phys. Rev. B **56**, 3360 (1997)
6. O. Gunnarsson, K. Schönhammer, Phys. Rev. Lett. **50**, 604 (1983); O. Gunnarsson, K. Schönhammer, Phys. Rev. B **28**, 4315 (1983)
7. M. Gamża, A. Ślebarski, H. Rosner, J. Phys.: Condens. Matter **20**, 025201 (2008)
8. A. Ślebarski, J. Spałek, M. Gamża, A. Hackemer, Phys. Rev. B **73**, 205115 (2006)
9. G. Venturini, B. Malaman, B. Roques, Mat. Res. Bull. **24**, 1135 (1989)
10. Y. Baer, G. Bush, P. Cohn, Rev. Sci. Instrum. **46**, 466 (1975)
11. K. Koepernik, H. Eschrig, Phys. Rev. B **59**, 1743 (1999)
12. J.P. Perdew, Y. Wang, Phys. Rev. B **45**, 13244 (1992)
13. H. Eschrig, *Optimized LCAO Method and the Electronic Structure of Extended Systems* (Springer, Berlin, 1989)
14. H. Eschrig, K. Koepernik, I. Chaplygin, J. Solid State Chem. **176**, 482 (2003)
15. D. Singh, *Plane waves, pseudopotentials and the LAPW method* (Kluwer Academic, 1994)
16. P. Blaha, K. Schwarz, G. Madsen, D. Kvasnicka, J. Luitz, *Program for calculating crystal properties* WIEN2k, Vienna University of Technology, 2001 (ISBN 3-9501031-1-2)
17. J.J. Yeh, J. Lindau, At. Data Nucl. Data Tables **32**, 1 (1985)
18. J.C. Fuggle, F.U. Hillebrecht, Z. Zolnierek, R. Lässer, Ch. Freiburg, O. Gunnarsson, K. Schönhammer, Phys. Rev. B **27**, 7330 (1983)
19. Y. Baer, R. Hauger, C. Zürcher, M. Campagna, G.K. Wertheim, Phys. Rev. B **18**, 4433 (1978)
20. A.J. Signorelli, R.G. Hayes, Phys. Rev. B **8**, 81 (1973)
21. S. Doniach, M. Šunjić, J. Phys. C **3**, 286 (1970)
22. S. Tougaard, P. Sigmund, Phys. Rev. B **25**, 4452 (1982)
23. M.P. Seah, W.A. Dench, Surf. Interface Anal. **1**, 2 (1979); J. Szajman, J. Liesegang, J.G. Jenkin, R.C.G. Leckey, J. Electron Spectrosc. Relat. Phenom. **23**, 97 (1981)
24. N. Witkowski, F. Bertran, D. Malterre, Phys. Rev. B **56**, 15040 (1997); N. Witkowski, F. Bertran, D. Malterre, J. Electron Spectrosc. Relat. Phenom. **117-118**, 371 (2001)
25. O. Gunnarsson, O. Jepson, Phys. Rev. B **38**, 3568 (1988)
26. A. Ślebarski, M.B. Maple, E.J. Freeman, C. Sirvent, M. Radłowska, A. Jezierski, E. Granado, Q. Huang, J.W. Lynn, Philos. Mag. B **82**, 943 (2002)
27. A. Ślebarski, A. Jezierski, A. Zygmunt, S. Mähl, M. Neumann, Phys. Rev. B **58**, 13498 (1998)
28. M. Gamża, A. Ślebarski, J. Deniszczyk, J. Phys.: Condens. Matter **20**, 115202 (2008)
29. N.D. Mathur, F.M. Grosche, S.R. Julian, I.R. Walker, D.M. Freye, R.K.W. Haselwimmer, G.G. Lonzarich Nature, **294**, 39 (1998); F.M. Grosche, M.J. Steiner, P. Agarwal, I.R. Walker, D.M. Freye, S.R. Julian, G.G. Lonzarich, J. Phys.: Condens. Matter **13**, 2845 (2001); S. Kawasaki, T. Mito, G.-Q. Zheng, C. Thessieu, Y. Kawasaki, K. Ishida, Y. Kitaoka, T. Muramatsu, T.C. Kobayashi, D. Aoki, S. Araki, Y. Haga, R. Settai, Y. Onuki, Phys. Rev. B **65**, 020504(R) (2001)
30. R. Yu, D. Singh, H. Krakauer, Phys. Rev. B **43**, 6411 (1991)
31. G. Venturini, B. Malaman, B. Roques, J. Less-Common Metals **152**, 185 (1989)
32. A.M. Boring, R.C. Albers, O. Eriksson, D.D. Koelling, Phys. Rev. Lett. **68**, 2652 (1992); J.F. Herbst, R.E. Watson, J.W. Wilkins, Phys. Rev. B **17**, 3089 (1978); J.F. Herbst, J.W. Wilkins, Phys. Rev. Lett. **43**, 1760 (1979); V.I. Anisimov, O. Gunnarsson, Phys. Rev. B **43**, 7570 (1991) and references there
33. J.W. Allen, S.-J. Oh, O. Gunnarsson, K. Schönhammer, M.B. Maple, M.S. Torikachvili, I. Lindau, Adv. Phys. **35**, 275 (1987); J.K. Lang, Y. Baer, P.A. Cox, J. Phys. F: Met. Phys. **11**, 121 (1981)
34. J.W. Allen, S.-J. Oh, I. Lindau, L.I. Lawrence, L.I. Johansson, S.B. Hagström, Phys. Rev. Lett. **46**, 1100 (1981); F. Patthey, J.-M. Imer, W.-D. Schneider, H. Beck, Y. Baer, B. Delley, Phys. Rev. B **42**, 8864 (1990); N. Witkowski, F. Bertran, T. Gourieux, B. Kierren, D. Malterre, G. Panaccione, Phys. Rev. B **56**, 12054 (1997)
35. M. Kohut, Int. J. Quantum Chem. **97**, 651 (2004); A.D. Becke, K.E. Edgecombe, J. Chem. Phys. **92**, 5397 (1990)